J. Fluid Mech. (1989), *vol.* 203, *pp.* 23–50
Printed in Great Britain

The transition to baroclinic chaos on the β-plane

By DANIEL R. OHLSEN† AND JOHN E. HART

Department of Astrophysical, Planetary, and Astrophysical Sciences, University of Colorado, Boulder, CO 80309, USA

(Received 25 July 1988 and in revised form 1 November 1988)

Experiments on two-layer β-plane flows are described. The regime diagrams for both easterly and westerly forcing indicate complex scenarios by which baroclinically unstable flows can become chaotic as the forcing is increased. The transition sequence can involve as many as three different vacillation mechanisms, but also exhibits the periodic window phenomena prevalent in many model dynamical systems. The fractal dimension of the chaos at low rotational Froude number F is measurable and is somewhat less than 3. The dimension increases as F is raised. A six-wave low-order model, while successfully predicting some of the observed vacillations, gives a relatively poor description of the chaos.

1. Introduction

There has been much recent study of the transition between ordered and chaotic states in fluid systems. Among those of geophysical interest, considerable recent work has focused on modulations and other types of nonlinear oscillations in baroclinically unstable systems. The annulus experiments of Buzyna, Pfeffer & Kung (1984) indicate that two types of vacillation precede the onset of chaotic motions as the basic rotation rate is increased. These two vacillations, amplitude and structural, also occur in the highly truncated model of Weng, Barcilon & Magnon (1986), the results of which bear some qualitative resemblance to the annulus experiments. The amplitude vacillation observed in the annulus appears to be of the energy-cycle type. Pedlosky (1970, 1971, 1972) developed a theory for this type of vacillation wherein the wave amplitude and the zonal flow periodically exchange available potential energy without an appreciable change of wave shape. The structural vacillation is a fluctuation in the shape of the wave field that is generated by the mixture of two radial modes with the same azimuthal wavenumber. The amplitudes of the two components of the travelling wave field are quasi-steady, but interference due to phase speed differences between the two generates a periodic tilting of the surface streamlines. In Weng *et al.*'s model these radial modes interact to produce a weak wavenumber zero (zonal flow) oscillation as well.

Hart (1985) studied the transition to chaos on the f-plane in a two-layer geometry. At small values of the rotational Froude number where azimuthal wavenumbers one and two are linearly unstable, the transition to chaos involves amplitude vacillation, with its characteristic strongly-coupled oscillations of a nearly single-component wave field and the zonal flow. The zonal flow oscillation period-doubled at least twice as the forcing was increased, and long-period chaotic oscillations appeared at small friction. Further decreases of friction did not produce a reverse cascade to a periodic or steady regime.

† Present address: Department of Physics, University of California, San Diego, La Jolla, CA 92093, USA.

In the two-layer geometry the structural vacillation is not likely to occur because the neutral curves for the linear eigenfunctions with the wavenumber/radial-modenumber pairs $(n, m) = (1, 1)$ and $(1, 2)$ are very far apart in parameter-space. That is, disturbances with the same wavenumber but two distinct radial modes are never close to being simultaneously neutral. For example, by the time the second radial mode of wavenumber-1 becomes neutral, the $(1, 1)$ disturbance is very unstable. So also are the higher wavenumber modes $(2, 1)$ and $(3, 1)$. This effect is illustrated in figure 2 for the β-plane. The f-plane result is similar (Hart 1985). Thus, in the two-layer experiments in a full cylinder the linear theory strongly suggests a competition between different wavenumbers of the lowest radial mode, not between two identical wavenumbers with different radial modes. Although these arguments would be strengthened by considering the stability of finite-amplitude steady-wave states to other modes, in fact the f-plane observations (e.g. Hart 1973) show several instances of 'wavenumber vacillation', which is precisely a periodic out-of-phase oscillation of the amplitudes of two different azimuthal wavenumbers, and no evidence of structural vacillation.

The two-layer model also lacks the potential for baroclinic interference vacillation between waves of the same azimuthal wavenumber but different *vertical* structures (and hence different phase speeds). This is simply because the two-layer model has the same vertical structure for all baroclinic waves. One needs to go to a three-layer model (Moroz & Brindley 1982) or to a continuous model with a nonlinear vertical basic stratification (Barcilon & Drazin 1984) in order to obtain interference oscillations of the type postulated by Lindzen, Farrel & Jacqmin (1982). There is the possibility of interference between barotropically unstable and baroclinically unstable modes. The measurement technique filters out barotropic modes, and the basic state is barotropically stable. Thus such an interference phenomena would be higher order than those produced by interactions between baroclinic modes.

However, recent observations and model calculations by Ohlsen & Hart (1988) have shown that a type of interference vacillation can occur in the two-layer system when the β-effect is significant. Two waves with different wavenumbers, different phase speeds, but the same radial cross-stream modal structure were predicted to coexist as a finite-amplitude mixed-wave equilibrium if β is large enough (Mansbridge 1984). This equilibration process would be the two-layer equivalent of wave dispersion in the annulus (e.g. Pfeffer & Fowlis 1968). Ohlsen & Hart show, however, that this equilibrium is always distorted by a low-frequency periodicity generated by the action of the nonlinearly forced sidebands of the fundamental dispersive waves, which can project onto the wavenumber zero zonal flow. The low-frequency vacillation occurs in the zonal flow as well as in the wave field, and typically increases in strength as the flow becomes more supercritical. No similar phenomenon has been observed on the f-plane, presumably because no (weakly nonlinear) mixed-wave states are permitted there (Hart 1981), except perhaps in the case of resonance where the double Hopf bifurcation analysis breaks down.

It thus appears that the β-plane two-layer geometry can contain at least two vacillatory phenomena: the normal amplitude vacillation, and the just mentioned 'nonlinear interference vacillation'. It is of interest to see how these may interact and become involved in the transition to chaos on the β-plane, and this is the main topic of the present paper. The two-layer geometry yields a consistent quasi-geostrophic β-plane, and results from laboratory experiments provide a useful calibration for theoretical and numerical models. In this spirit, a short discussion of some low-order model results is given at the end of the paper. The main focus is, however, on the

intricate interweaving of periodic and chaotic motions as the friction parameter is changed, on the differences between the response of the system for easterly and westerly forcing, and on the low-dimensional (but still unexplained) nature of the chaos observed at low rotational Froude numbers.

The paper is organized as follows. Section 2 describes the experimental technique, and §3 outlines the experimental results, concentrating on a few typical examples of multiply periodic flows. Section 4 describes some evidence for the existence of low-order attractors. This is followed by a discussion of the numerical model results and a statement of the conclusions.

2. Experimental procedures

The cross-section of the full-cylinder experiment is shown in figure 1, and the experimental data is given in table 1. The fluids are a low-viscosity silicone oil (top) and a water–methanol mixture (bottom). The basic rotation is chosen so that the parabolic interface equilibrium in the absence of driving is exactly half as strong as the lid parabola. Thus vertical vortices in both layers are stretched as they are displaced radially outwards and this gives the β-effect. The topographic β-effect has a magnitude of

$$\beta' = \frac{d}{2H_i} = 0.239,$$

where d is the extent of the upper lid parabola and H_i is the layer depth(s). In geophysical applications β has the same significance as the non-dimensional β-parameter

$$\beta_g = \frac{\cos(\theta)L}{R_p},$$

where θ is the latitude, L the channel width or horizontal lengthscale of the phenomenon, and R_p is the radius of the planet. The laboratory value is thus typical of many geophysical flows.

A number of constant parameters are given in table 1. Obviously the lid geometry fixes the equivalent β-effect, and the viscosity parameter χ, being proportional to the square root of the viscosity ratio, is nearly constant, even as the methanol concentration is changed slightly to vary the density ratio. The equilibrium depths H_1 and H_2 are set equal to within 1%. The variable parameters are the rotational Froude number

$$F = \frac{4\Omega^2 L^2}{g' H_1}, \tag{1}$$

and the friction parameter

$$Q = \frac{(\nu_1 \Omega)^{\frac{1}{2}}}{\omega H_1}, \tag{2}$$

which is essentially the ratio of the square root of the Ekman number to the Rossby number based on the differential rotation ω. In (1) g' is the reduced gravity $g\Delta\rho/\bar{\rho}$.

There are three small resistance measuring probes placed along a diameter. Each probe is a 0.003 in. wire stretched through the interface between the silicone oil and methanol–water mixture. Two probes are at radii of $r = 0.74L$ and located at opposite sides of the tank. The third is on the axis. The 'axis-probe' measures only the zonal flow component of the height field, because all components of a Fourier–Bessel expansion of the interface height with wavenumber greater than zero vanish at $r = 0$. The off-axis 'wave-probes' can be summed or subtracted to give the

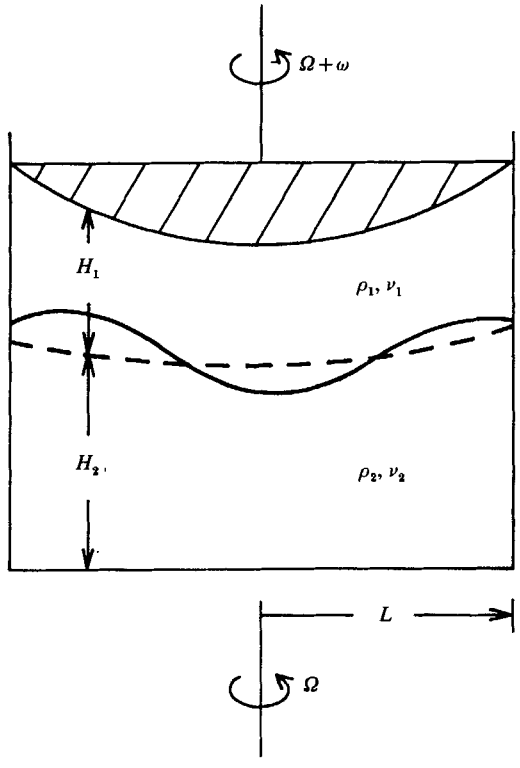

FIGURE 1. Cross-section of the two-layer system. The dashed lines show the locations of the interface height probes. See table 1 for definitions and values of the various parameters.

contributions of the even or odd non-zero wavenumbers. All three probes are elements of individual a.c.-brides, and operate simultaneously on their own separate carrier frequencies. The outputs are bandpassed filtered to eliminate cross-talk. Ohlsen (1988) provides further experimental details.

Experiments are carried out in a quasi-static run-up or run-down mode. The basic rotation (about 2 s per revolution) is established and the differential rotation ω is set so that Q is in the axisymmetric regime. The differential rotation is stepped by 1–5% every 2–4 h so that over a period of several days a traverse is made through decreasing Q at constant F. For some runs Q is then slowly increased from low values out into the axisymmetric regime. Then the methanol–water fluid density is changed slightly to attain a new Froude number and another experiment is run. The experiments were controlled by a PDP1123 computer and the probe data were digitized and logged on tape for future processing.

The major experimental limitation (apart from time) is that small fluctuations in the basic rotation (of order a few tenths of a percent), as well as long-time room temperature changes that affect the Froude number and the electronics, limit the effective resolution in Q to about 1%. The bifurcation structure of the β-plane flows may indeed be more complex than illustrated here, but we feel confident that it is not less complicated. That is, further stability in the experiment would not remove any of the regimes reported here. That the different types of motions shown in §3 occur for both increasing and decreasing Q (without significant hysteresis), and that similar

Dimensional parameters	
$H_i = 13.0$ cm	mean depth of each layer
$L = 22.54$ cm	radius of cylinder
ρ_i g/cm^3	fluid density
ν_i cm^2/s	kinematic viscosity
$g = 979.6$ cm/s^2	gravitational acceleration
$d = 6.23$ cm	depth of lid parabola
$\Omega = 3.465$ rad/s	basic rotation
ω rad/s	differential rotation
Coordinates	
r	non-dimensional radius, scaled by L
θ	azimuthal (polar) angle
u_i	radial velocity, scaled by $L\omega$
v_i	azimuthal velocity, scaled by $L\omega$
t	time, scaled by ω^{-1}
Non-dimensional parameters	
$\beta = d/H_1$	planetary vorticity gradient
$\Delta\rho/\bar{\rho} = 2(\rho_2-\rho_1)/(\rho_2+\rho_1)$	stratification
$\chi = (\nu_2/\nu_1)^{\frac{1}{2}}$	viscosity ratio
$K = H_1/H_2$	depth ratio
$\epsilon = \omega/2\Omega$	Rossby number
$E = \nu_1/2\Omega H_1^2$	Ekman number
$Q = (\frac{1}{2}E)^{\frac{1}{2}}/\epsilon$	friction parameter
$F = 4\Omega^2L^2/g(\Delta\rho/\bar{\rho})H_1$	Froude number

TABLE 1. Basic parameters and scaling for experiment and model. The top layer is denoted by $i = 1$, and the bottom by $i = 2$.

structures usually span more than one adjacent value of F, indicate that the observations are reasonably robust.

3. Experimental results

Figure 2 is one main result of this study. It shows the locations of the various regimes on the β-plane for easterly forcing, $\omega < 0$. Runs were done at the constant values of F indicated by the arrows at the right-hand side of the graph. The density of points along each track is much higher due to the 1–5 % steps in Q. No significant hysteresis was noticed, on increasing or decreasing Q, even for the periodic windows to be illustrated below.

There is baroclinic instability for easterly forcing in the experiments, as illustrated by the favourable comparison between the observed transition from axisymmetric to wavy flow and the theoretical predictions from a two-layer quasi-geostrophic model (thin lines). In fact, in the two-layer model with a solid rotation basic state there is no difference in the linear neutral curves for easterly and westerly forcing for K, $\chi \approx 1$ (the equations are shown in Ohlsen & Hart 1988).

Summarizing the situation, at low F where azimuthal wavenumber-1 is the only unstable linear mode, there is no nonlinear interference vacillation (NIV). The periodic regions are dominated by amplitude vacillations that have lower frequencies than the NIV. On the left-hand side of the NIV region at larger F the higher

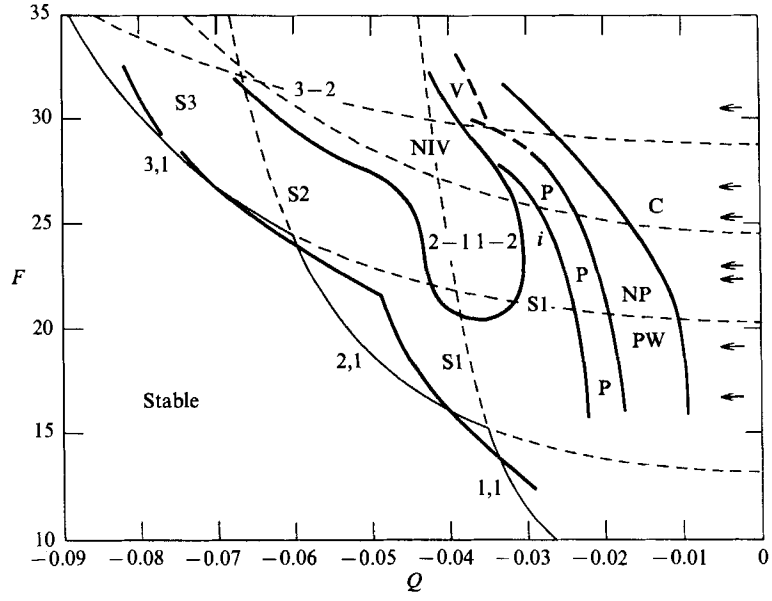

FIGURE 2. Regime diagram for easterly forcing on the β-plane. Sn denotes a steady wave with azimuthal wavenumber n, NIV denotes nonlinear interference vacillation, P denotes singly periodic amplitude vacillation, NP denotes noisy periodicity, and PW denotes periodic windows. V is a narrow region of wavenumber vacillation, and C is a chaotic region without a dominant periodicity. The thin lines illustrate the linear neutral curves with the wave and mode numbers shown.

wavenumbers dominate the wave field. On the more strongly forced right-hand side the opposite is true. In fact for moderate F the NIV gives way to a steady wavenumber-1 flow at fairly high supercriticality. The P-region is singly periodic. But within the NP/PW region there are complex periodicities intermixed with chaos. Rather than clutter up the diagram with more regions, we give a set of examples that are intended to characterize the types of motions observed in these β-plane experiments.

Figure 3 illustrates the amplitude vacillation of a single-wavenumber at low F. Subtracting and adding the two wave-probes indicates that the odd azimuthal wavenumbers (dominated by $n = 1$) have 8 times the amplitude of the even waves (dominated by $n = 2$). Note that the frequency of the modulation is about 0.05, or roughly twenty lid-periods per cycle. The electronics and plots are set up so that the most positive excursions of the axis-probe correspond to the weakest zonal flow baroclinicity (but note that for positive Q the opposite is true). Therefore it is seen that the wave amplitude maxima are positively correlated with the zonal baroclinicity minima (the source of the baroclinic instability). This is another signature of the amplitude vacillation where the waves and zonal flow exchange available potential energy.

As $-Q$ decreases the amplitude vacillation in figure 3 period doubles, then becomes chaotic. An example is shown in figure 4. Note that figure 4(a) shows a single spike at a frequency of about 0.04 that is more than a factor of 10^4 above the background. We call this a monochromatic (period-1) vacillation. Figures 4(b) and 4(c) show a period-2 vacillation and a noisy-periodic state respectively. In figure 4(c) the

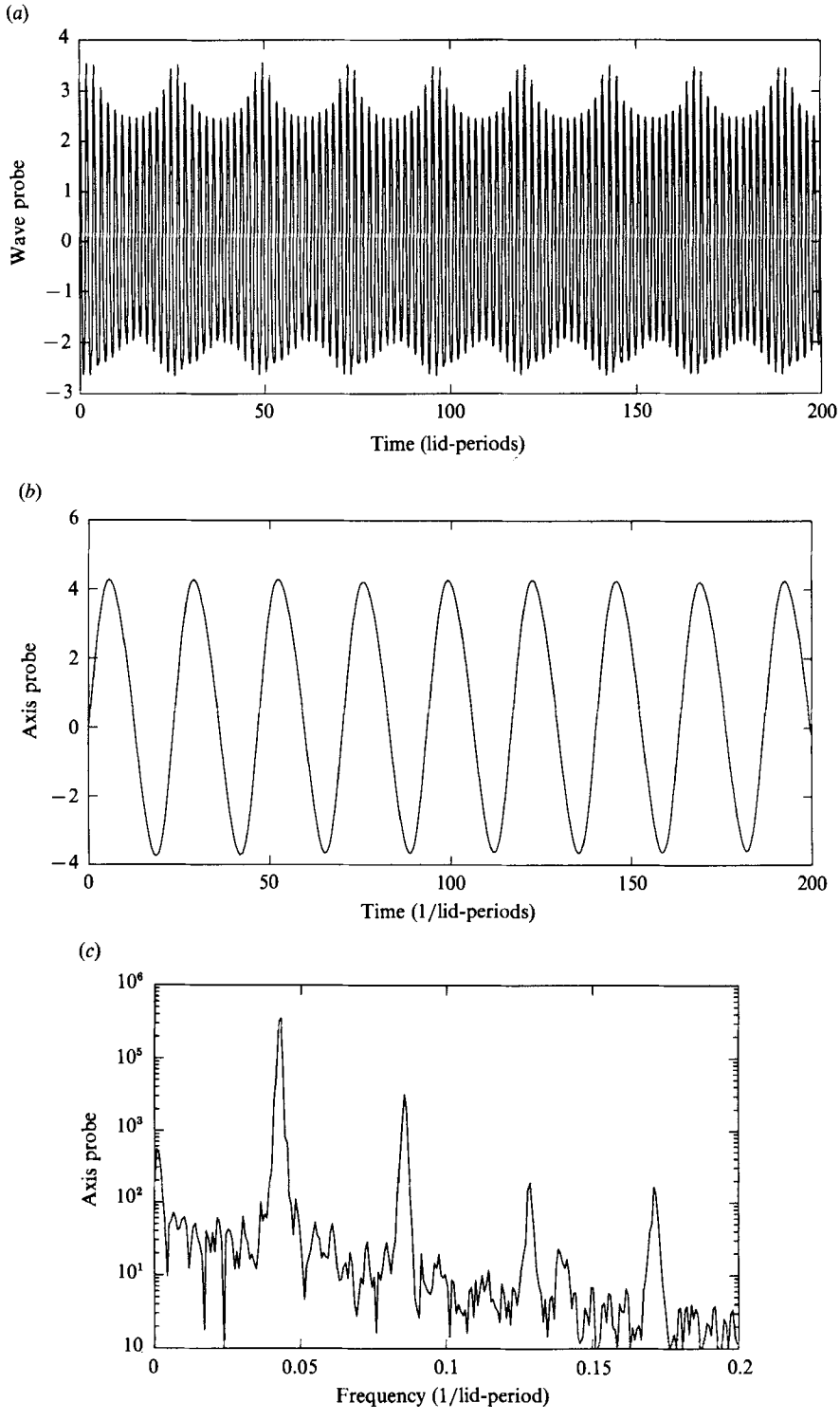

FIGURE 3. Data at $F = 16.7$, $Q = -0.224$. (*a*) shows the wave probe, (*b*) the axis probe and (*c*) the spectrum of the axis-probe signal.

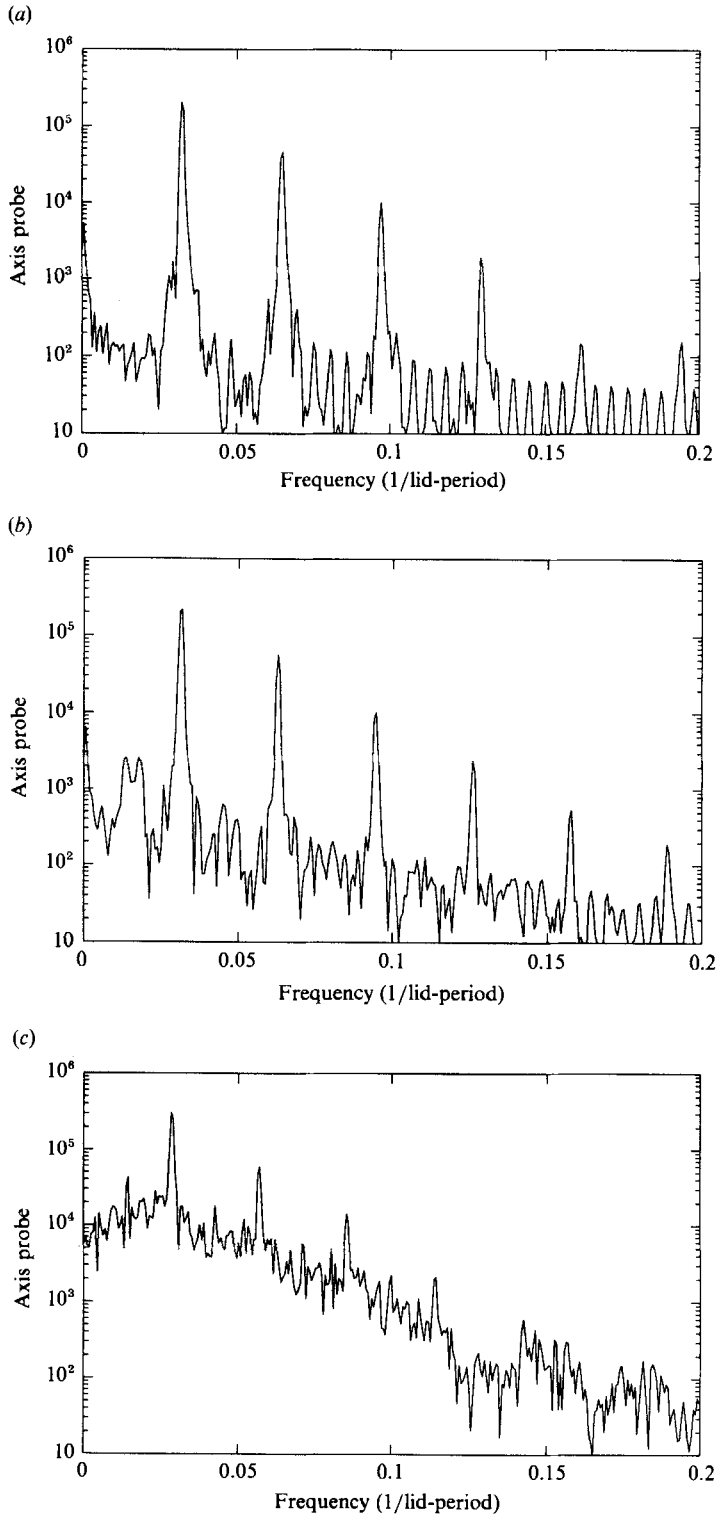

FIGURE 4. Spectra of the axis probe at $F = 16.7$. In (*a*) $Q = -0.0201$, in (*b*) $Q = -0.0199$, and in (*c*) $Q = -0.0189$.

background broadband component of the spectrum has risen by a factor of 100 over the measurement background.

As $-Q$ decreases further the broadband rises slightly until $Q = -0.0142$, where a stable period-3 zonal flow orbit is observed (figure 5*a–c*). The wave-probe would show a period-3 2-torus as the travelling-wave frequency is incommensurate with the zonal vacillation. On the more inviscid side of the period-3 response is a weakly chaotic period-2 regime that retains weak vestiges of period-3 (figure 5*d–e*).

This noisy periodicity continues until $Q = -0.0115$ when the period-2 signal becomes very large and the system settles into a periodic orbit. Figure 6 shows what this looks like. By frequency tracking with Q we can tell that the 0.036 peak is the fundamental and the sub-harmonic at about 0.018 is simply very strong. It can be seen that the minima of the zonal flow time trace (the maximum zonal baroclinicity) coincide almost exactly with the minima of the wave envelope, again a characteristic of energy-cycle amplitude vacillation.

With more driving the spectra show an elevation of the background and a broadening of the main peaks of figure 6(*c*) without any obvious further period-doublings. This is illustrated better in §4, where it is also suggested that the chaos here is relatively low-dimensional. Figure 7 shows what the various signals look like at slightly smaller $-Q$.

At $F = 25.4$ a broad regime of nonlinear interference vacillation (NIV) intrudes into the steady wave regime. NIV is discussed in detail in Ohlsen & Hart (1988). We give one example here in order that we may compare its characteristics with those of amplitude vacillation. Figure 8(*a*) shows a typical time-trace of a wave-probe during NIV. Figure 8(*b*) shows that this time-trace is made up of two fundamental waves with different (non-resonant) frequencies f_1 and f_2 and wavenumber $n_1 = 1$ and $n_2 = 2$. The nonlinear interaction of the two fundamentals produces an azimuthal wavenumber-1 sideband with frequency $f_2 - f_1$. This nonlinear product can then interact back with the wavenumber-1 fundamental (actually with its conjugate), to give a zonally invariant response forced at the NIV frequency $f_2 - 2f_1$, or equivalently, $2f_1 - f_2$. This vacillation frequency dominates the zonal flow response (figure 8*c*), but also shows up as a modulation frequency for the wave field itself. The NIV frequency is a factor five or so higher than typical amplitude vacillation frequencies in these experiments.

As Q changes the relative frequencies $f_1(Q)$ and $f_2(Q)$ also change, so that for some points in parameter space $2f_1 - f_2$ can be close to a low-order rational fraction of f_1 (or f_2). Figure 9 shows an example where $2f_1 - f_2$ happens to be equal to $0.2 f_1$ (within the resolution of the experiment). Plots of the frequency ratio *vs.* Q (not shown) indicate that there may be a flattening near $f_2 f_1^{-1} = 0.5$. Such a flattening would imply a frequency entrainment. However the current data points were not sufficiently close (in Q) to unambiguously resolve this question, for the frequency locking, if it exists, occurs over a narrow band of Q.

As $-Q$ decreases towards the right-hand side of the NIV region, wavenumber 2 gets weaker and wavenumber 1 gets stronger. This reflects a tendency for the preferred wave at a particular F to have a wavelength longer than that suggested by the linear neutral curves (e.g. Hart 1981). There is then a band of steady states, involving a dominance of wavenumber 1, sandwiched between the NIV region and the longer-period amplitude vacillation region which occurs at smaller Q.

Further decreases of $-Q$ towards the inviscid limit ($Q = 0$) bring the system into amplitude vacillation. The transition sequence proceeds then more or less as at $F = 16.7$, except that a weak quasi-periodicity was observed over values of Q surrounding

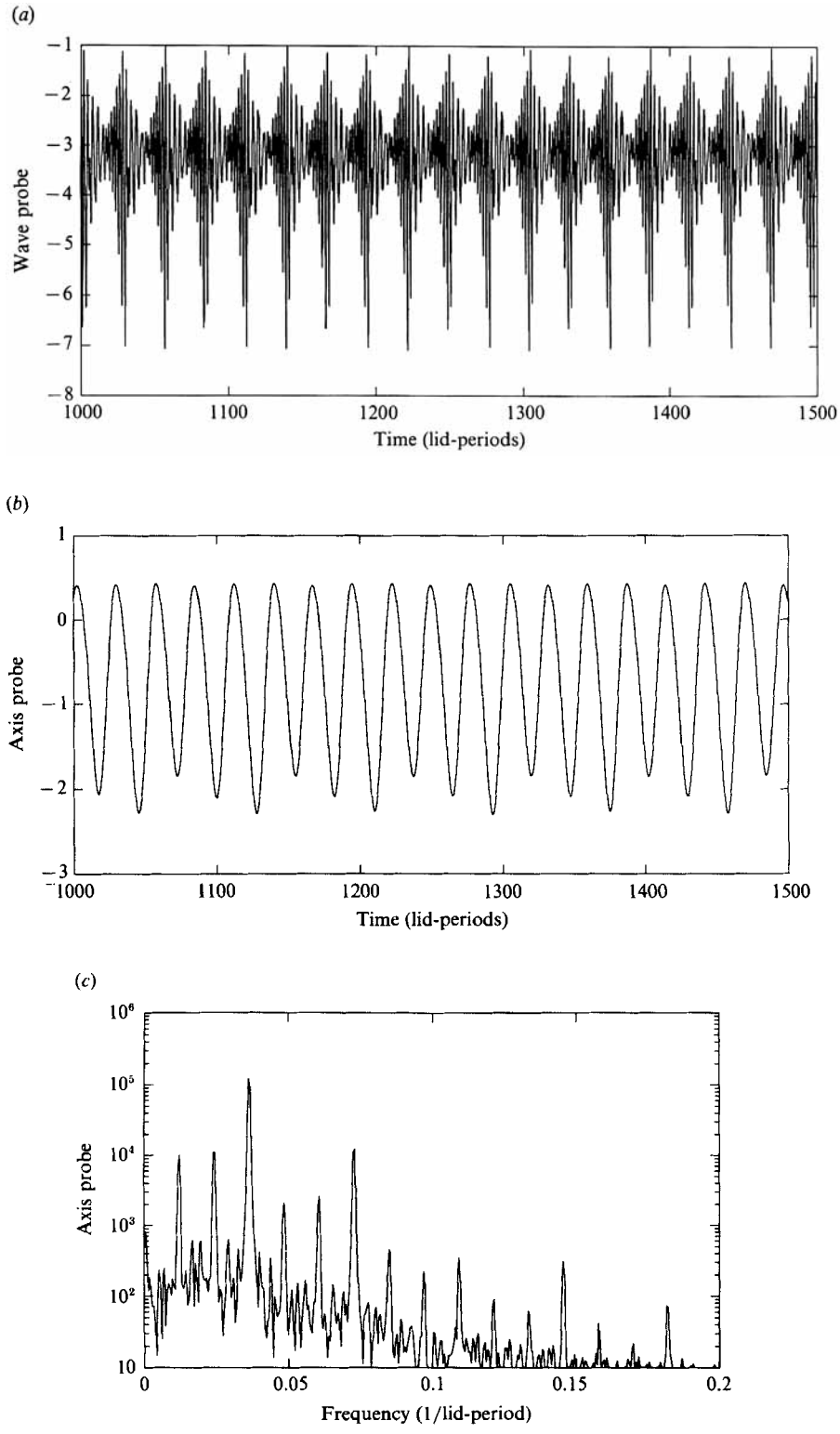

FIGURE 5(*a–c*). For caption see facing page.

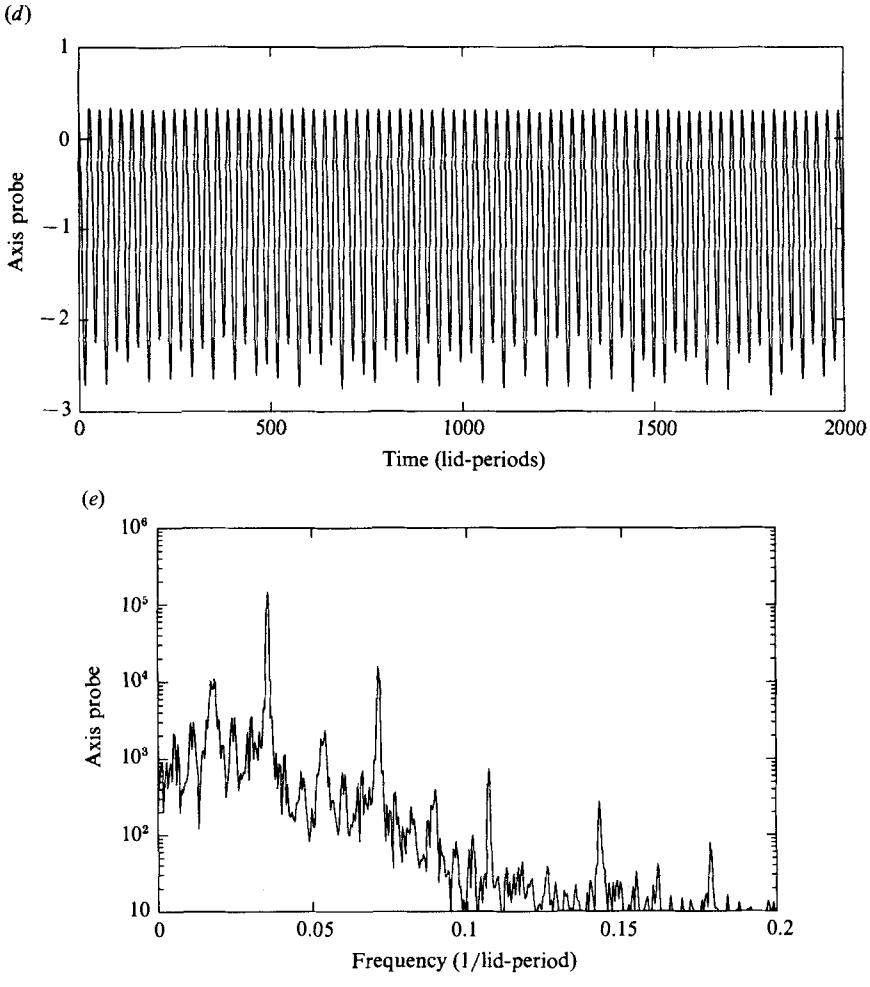

FIGURE 5. Period-3 response at $F = 16.7$, $Q = -0.0142$. (*a*) shows the wave probe, (*b*) the axis probe, and (*c*) the axis-probe frequency spectrum. At slightly smaller Q the system becomes noisy. In (*d*) the axis probe is shown for $Q = -0.0139$, and (*e*) shows its frequency spectrum.

-0.0227. This is illustrated in figure 10. It is not known whether this might have been experimentally induced. It persists from -0.0227 to -0.0213 and causes the period-3 response at -0.0222 and the period-2 response at less negative Q to breathe in and out slightly at the very long modulation frequency (0.007).

Figure 11 shows a highly chaotic state and illustrates the much broader axis spectrum typical of the region outside the noisy-periodic band. The negative correlation between the axis-probe and the envelope of the waves is still strong.

At $F = 30$ evidence was found for a sort of wavenumber vacillation. This was somewhat surprising because we had expected to see a region where the NIV and amplitude vacillation regions overlapped to produce a 2-torus on the axis (as in the model, see below). Instead the processes that maintain the mixed-wave NIV regime appear to break down, but instead of leading to a steady single-wave state, the two waves vacillate. This is shown in figure 12. There again is the correlation with the minima of the axis signal and the minima of the wave envelope. The axis spectrum is dominated by a low-frequency 0.048. Just to the left in parameter space, at

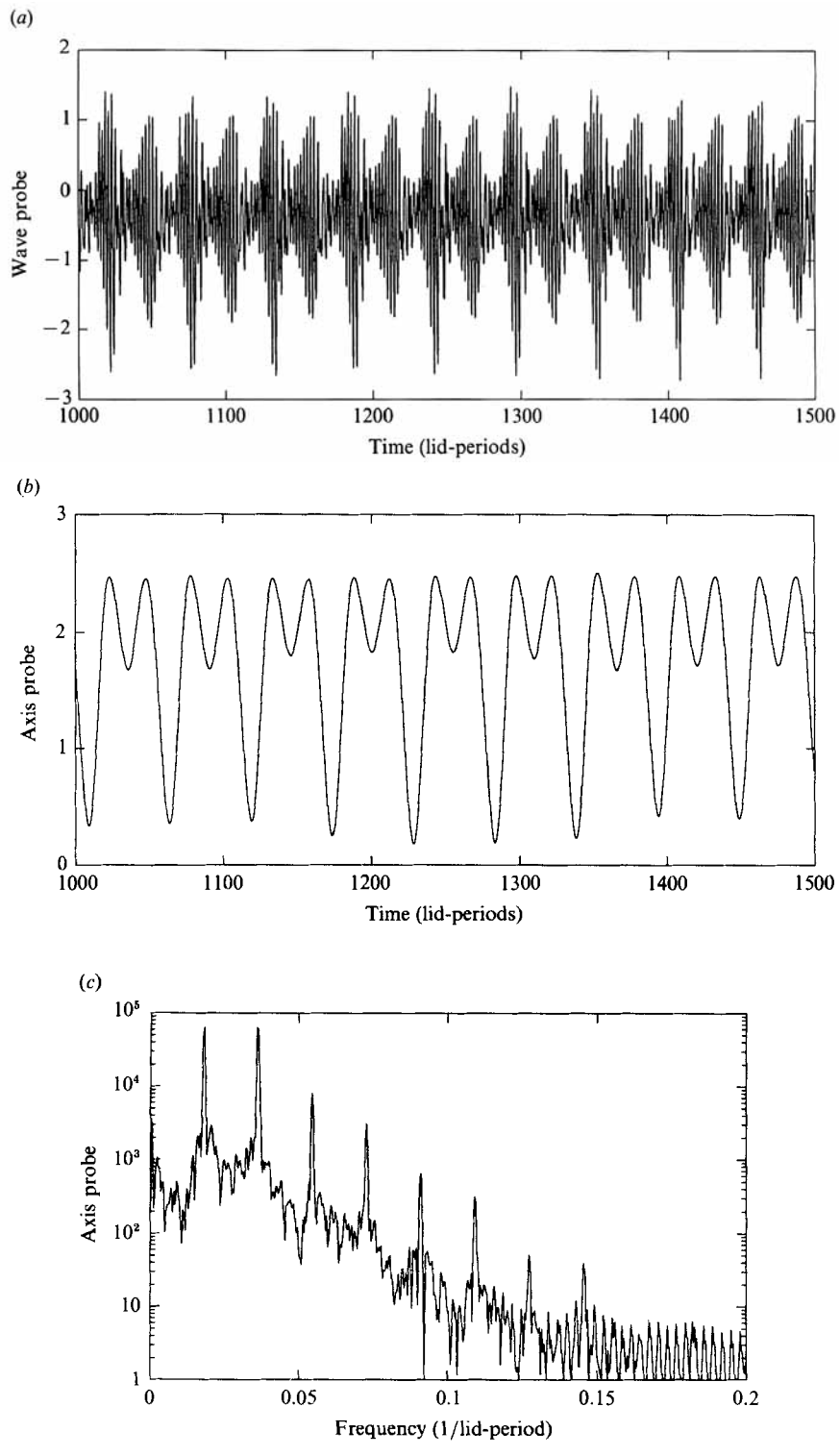

FIGURE 6. Strong period doubling at $F = 16.7$, $Q = -0.0115$. (*a*) is the wave probe, (*b*) the axis probe, and (*c*) the axis-probe spectrum.

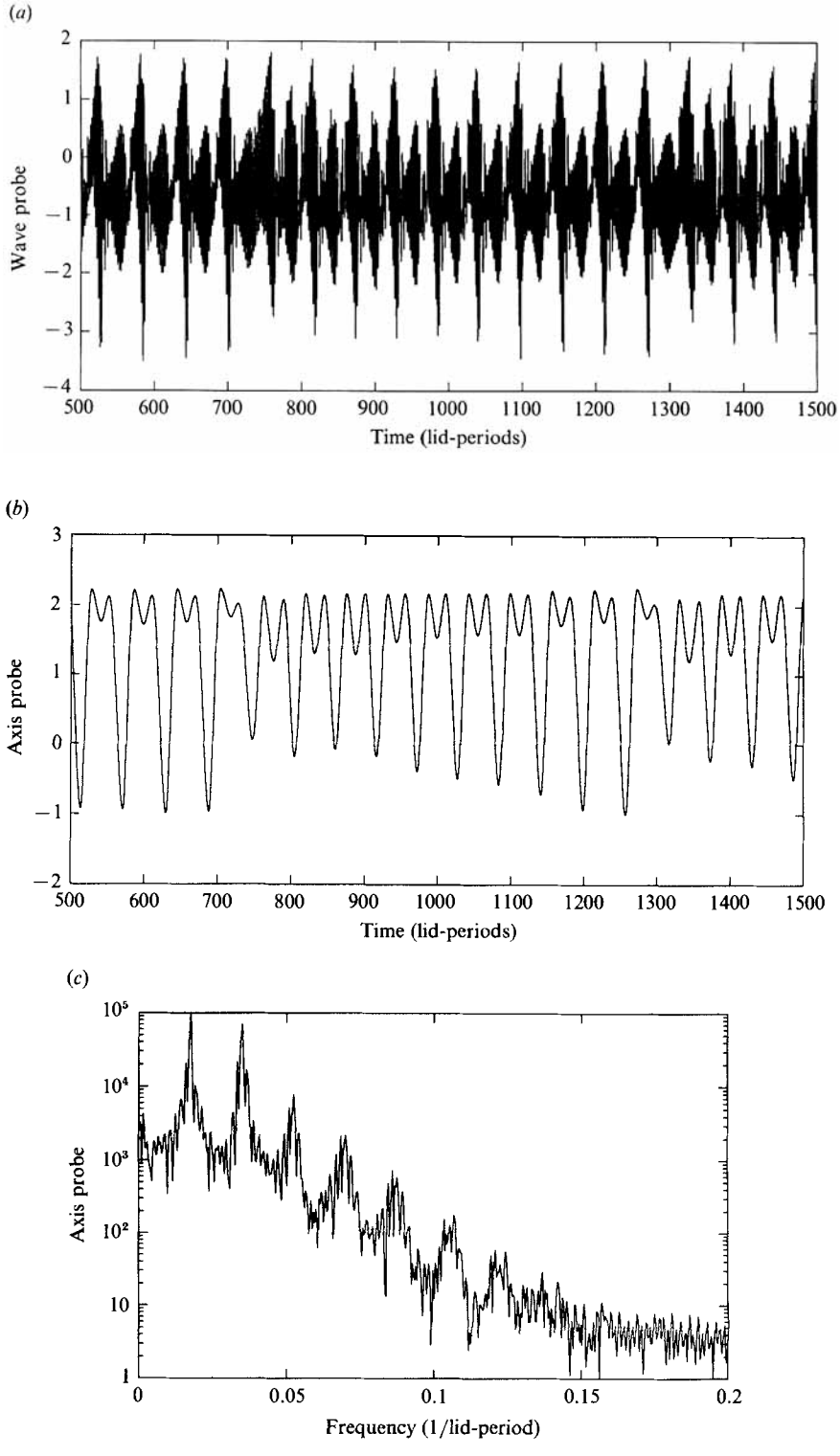

FIGURE 7. Noisy periodic chaos at $F = 16.7$, $Q = -0.0112$. (*a*) is the wave probe, (*b*) the axis probe, and (*c*) the axis-probe spectrum.

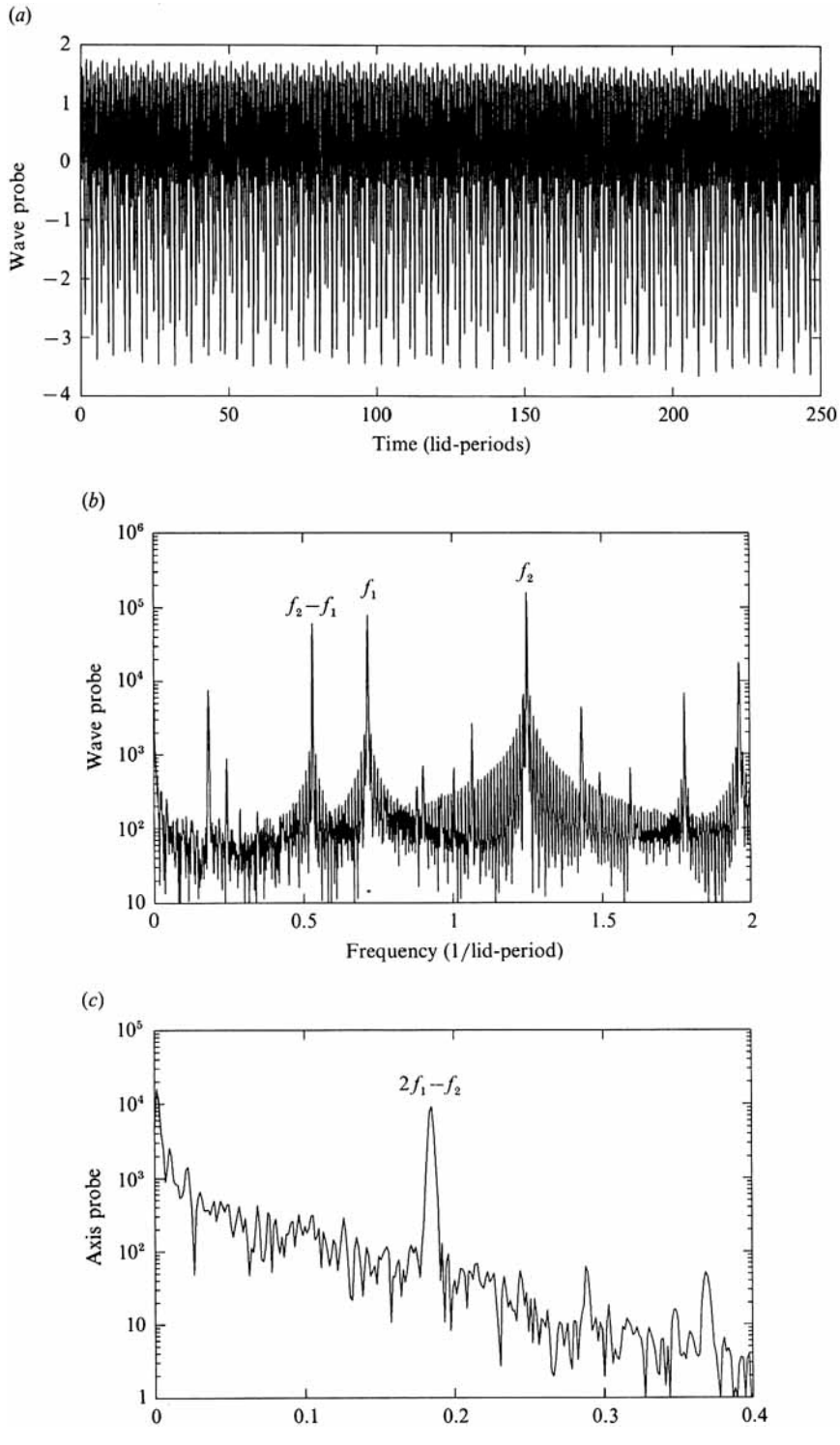

FIGURE 8. A nonlinear interference vacillation. $F = 25.4$, $Q = -0.0412$. (*a*) is the wave probe, (*b*) the wave-probe spectrum, and (*c*) the axis-probe spectrum.

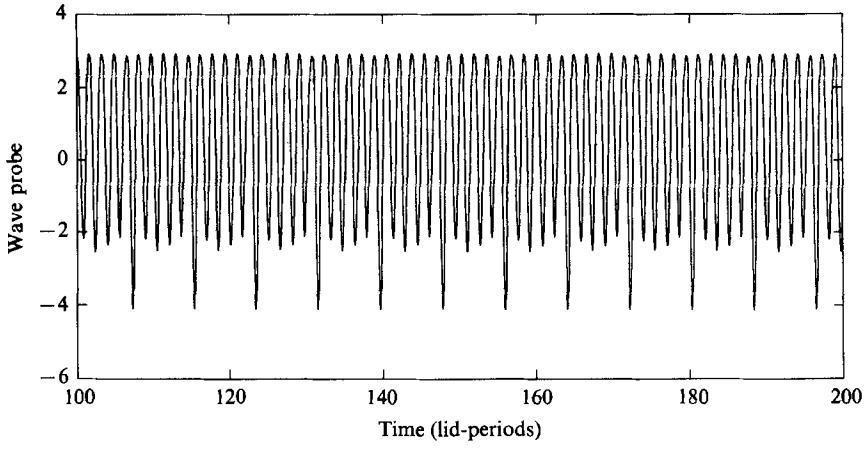

FIGURE 9. Phase-locked interference vacillation. $F = 25.4$, $Q = -0.0324$.

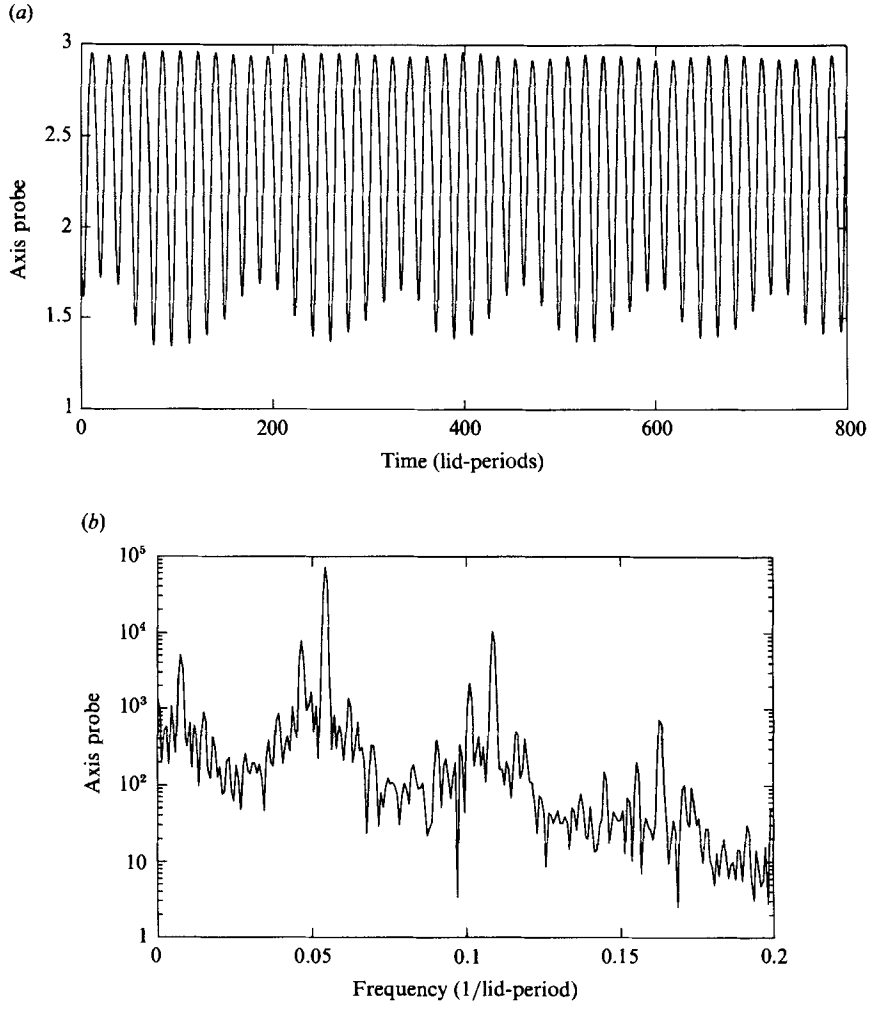

FIGURE 10. Quasi-periodic flow. $F = 25.4$, $Q = -0.0227$. (a) is the axis probe and (b) is its spectrum.

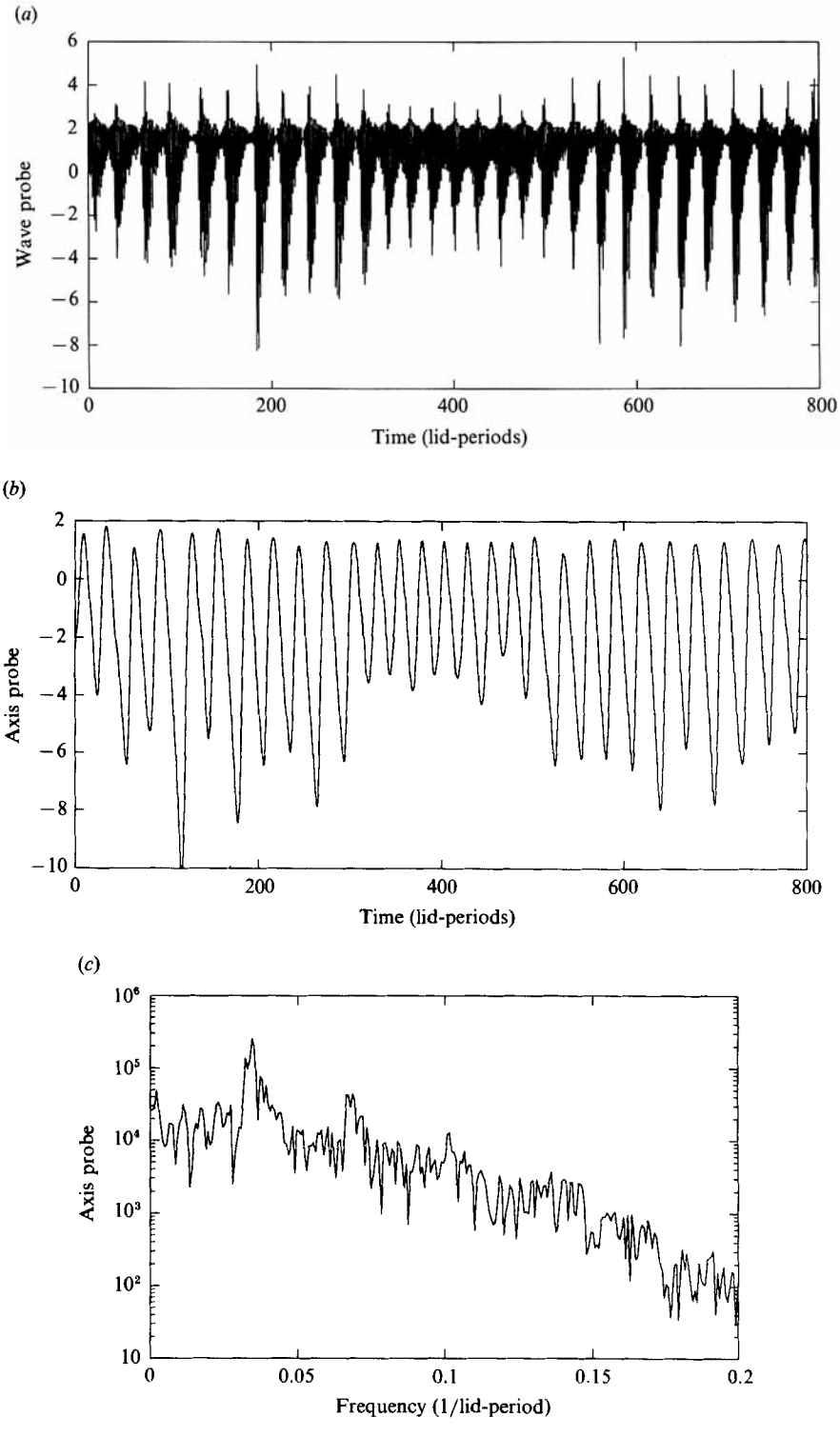

FIGURE 11. Highly chaotic flow. $F = 25.4$, $Q = -0.0211$. (*a*) is the wave probe, (*b*) is the axis probe and (*c*) is the axis-probe frequency spectrum.

$Q = -0.045$, the NIV axis frequency is 0.456 or $3f_2 - 2f_3$. Figures 12(*c*) and 12(*d*) show the even and odd wavenumbers. The odd ones, mostly low-frequency wavenumber 1, modulate in quadrature with the even ones in a manner typical of models and other experiments showing wavenumber vacillations (e.g. Hart 1973). That is, wavenumber-2 has maximum amplitude when wavenumber-1 is at a minimum, and vice versa.

Figure 13 shows the regime diagram for westerly ($\omega > 0$) forcing. Although the gross structure including the location of the periodic, noisy periodic, and chaotic regions is similar, there are several major differences between this regime diagram and that for easterly forcing. The NIV region is pushed to much higher F values. The NIV regime at lower F with easterly forcing is replaced by a steady phaselocked state (L) that gives way to an amplitude vacillation that involves *both* wavenumber 1 and wavenumber 2, which are locked in phase.

Figure 14 illustrates these phaselocked states. Figure 14(*a*) shows the time trace of a steady state in which wavenumber 1 and wavenumber 2 propagate around the tank in concert. The phase speeds are the same and there is no interference vacillation. As Q decreases the amount of wavenumber 2 in the steady states does not decrease, relative to wavenumber 1, as it typically does for easterly forcing. A phaselocked amplitude vacillation is shown in figure 14(*b*). This is illustrated in figures 14(*c*) and 14(*d*) where it is seen that the even wavenumbers (principally number-2) dominate this vacillation which is occurring on the boundary between single-period and period-doubled response. During the vacillation the envelopes of the odd and even wavenumbers modulate simultaneously and in phase. The total wave amplitude is large when the zonal baroclinicity is small.

Figure 15 gives a last example of a period-doubling transition to chaos. In this period doubling sequence wavenumber-2 dominates the non-zonal field. The wave attractors in this cascade are a sequence of period-doubled tori. A period-4 limit cycle is evident in the zonal response, but period-8 is not clearly observed. This could be due to its absence so that the transition sequence is made of a finite three-step period-doubling. On the other hand, the period-8 component might be too small in the face of measurement noise and small undesired parameter variations. This issue can only be addressed with a better controlled experiment. In a manner similar to the situation for easterly forcing, the chaos that results from this period-doubling cascade is broken, as Q is decreased, by a period-3 window, occurring here at $Q = 0.0267$.

4. Low-dimensional attractors

Lorenz (1963) introduced the idea of reducing the study of a differential system to a mapping made from the maxima or minima of the zonal flow correction (in his problem the zonally averaged temperature was used). This mapping is equivalent to a Poincaré section. It is possible to repeat Lorenz's procedure to investigate the structure of hopefully low-dimensional mappings that might result from the data if the original dynamical system is of reasonably small dimension.

Figure 16 shows four 'min-maps' constructed for several values of Q at $F = 16.7$ in the noisy period-2 regime. The maps indicate a broadening of the two minima clumps associated with period-2 at -0.0113, but along a curve which develops into a rounded map similar to those of Hart (1986), who studied the effect of physical asymmetries on the original Lorenz cusp-map. The qualitative agreement is most

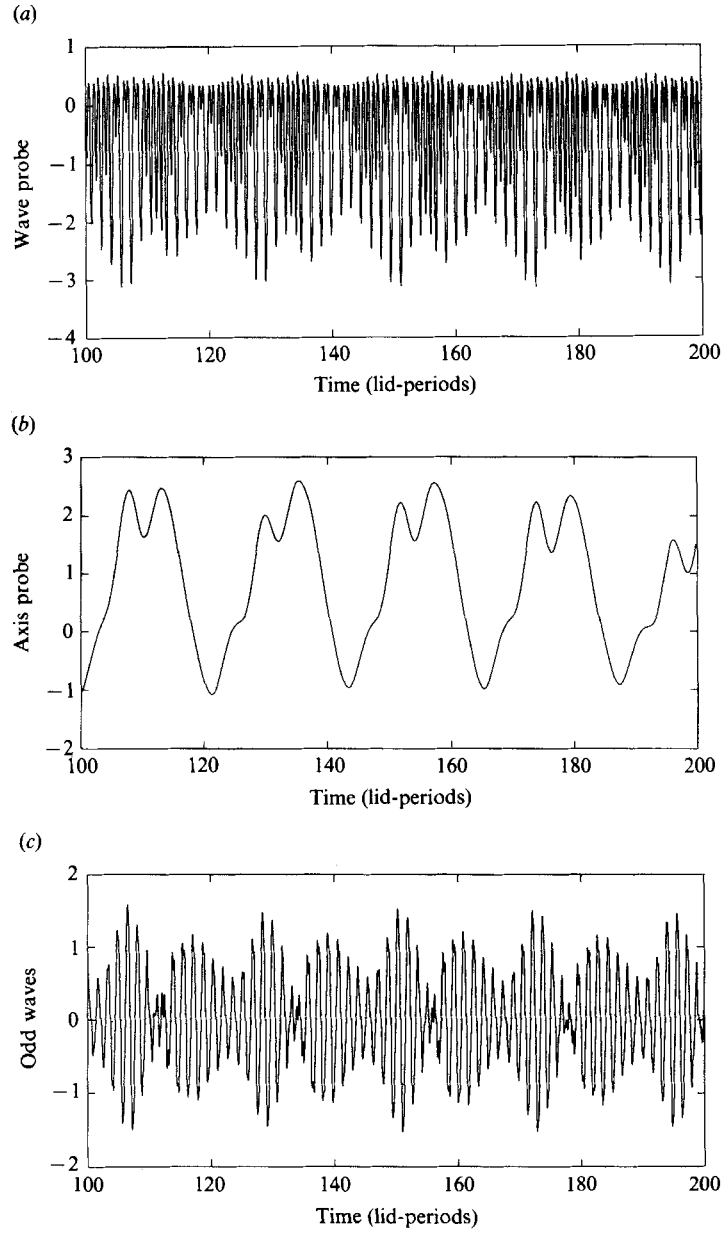

FIGURE 12(*a–c*). For caption see facing page.

likely coincidental, but maps with similar shapes have often been found associated with low-dimensional chaos in model systems.

The lower bound on the fractal dimension or capacity can be estimated from a data set by calculating the correlation dimension of Grassberger & Procaccia (1983*a*, *b*, *c*). The details of this computation are given in Ohlsen (1988). Table 2 shows the dimension estimates. For observed *periodic flow* on the axis with $F = 17$ and $Q = -0.022$, -0.020, and -0.013 (period-3) the correlation dimensions are near 1.0. Of course the wave field adds one additional dimension so the system correlation

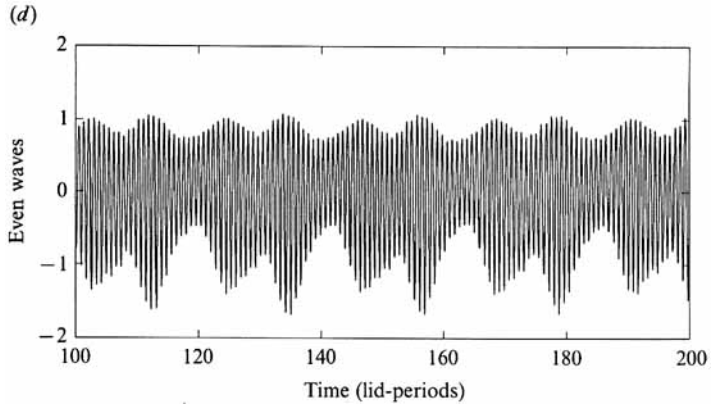

FIGURE 12. Wavenumber vacillation at $F = 30.7$, $Q = -0.0412$. (*a*) is the wave probe, (*b*) the axis-probe, (*c*) the difference of the two wave probes (the odd wavenumbers) and (*d*) the sum of the two wave-probes (the even wavenumbers).

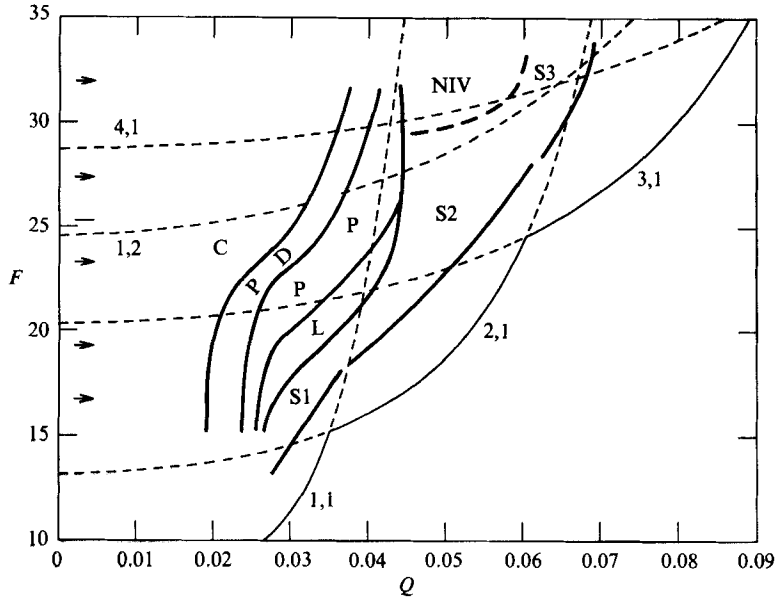

FIGURE 13. The regime diagram for westerly forcing. The notation is the same as in figure 2 with the addition that L refers to a phase-locked vacillation.

dimension is near 2.0. That is, the wave-probe mapping is two-dimensional (a 2-torus), precisely what one would expect because the travelling-wave frequency is incommensurate with the energy-cycle modulation. The relatively low dimensions of the flows at low F agree with the organized structure of the mappings in figure 16. The dimensions of the underlying chaotic attractors for the whole system are bounded below by a number of order 2.5 ± 0.2 when $F = 17$ and $-Q > 0.01$. At higher F, however, the dimensions are larger. Unfortunately the data are such that reliable dimension estimates can only be obtained if the *zonal-flow* dimension is less than about 2.5. It would be most interesting to determine how fast the dimension increases with F over a larger range, and thus to estimate what magnitude it might

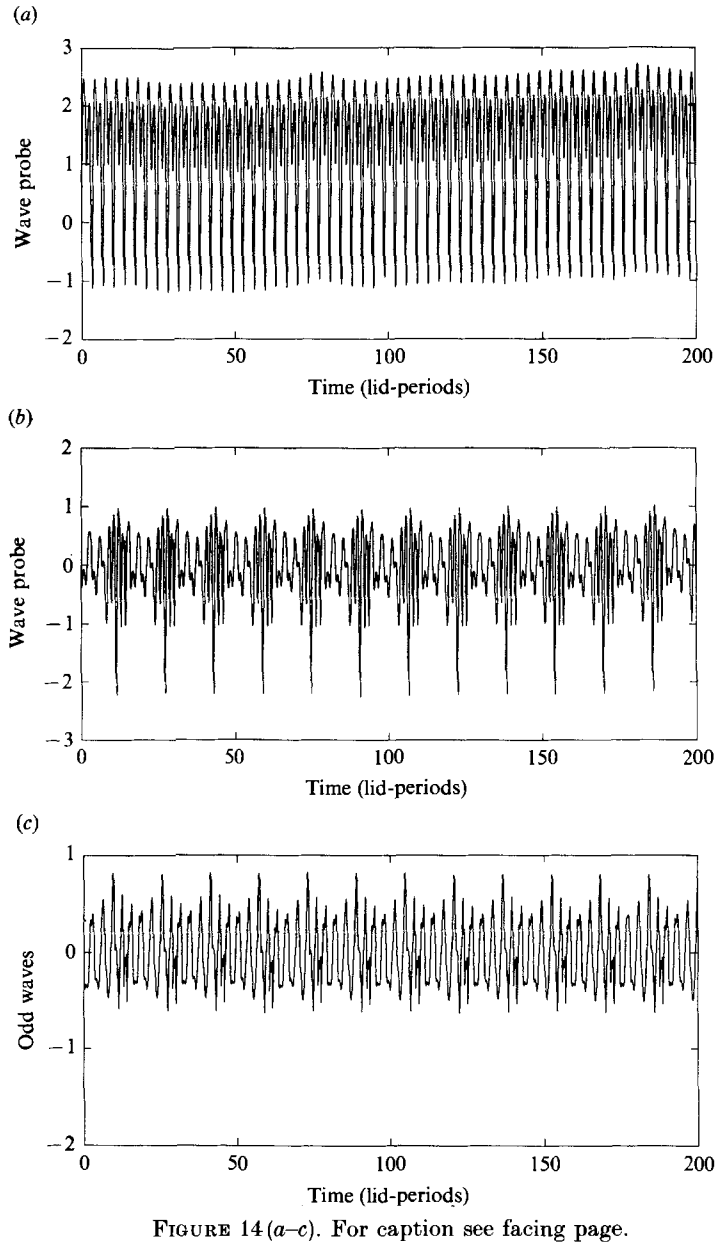

FIGURE 14(*a–c*). For caption see facing page.

take for F-values more appropriate to the atmosphere (around 50) or the ocean (around 250). In practice, such a determination is as yet impossible. Almost infinite precision and measurement time would be required.

5. Spectral model predictions

The laboratory results were compared with results from a low-order numerical model. This model is described in Ohlsen & Hart (1988) and more completely in Ohlsen (1988). It is a quasi-geostrophic two-layer model on the (topographic) β-plane with top, bottom, and interfacial Ekman layers. A spectral expansion is made in

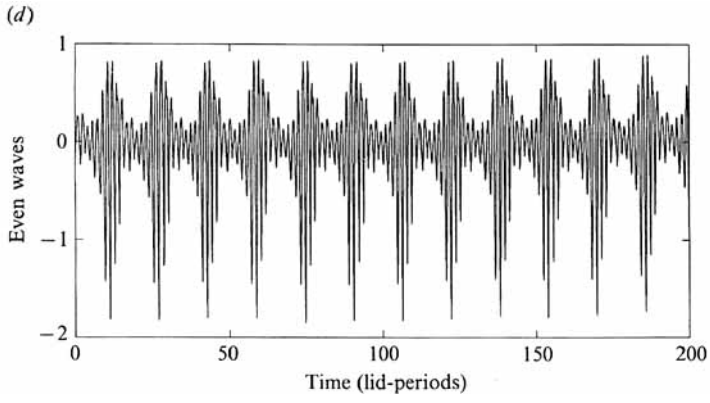

FIGURE 14. Phase-locked steady waves at $F = 23.2$, $Q = 0.412$ (*a*), and phase-locked vacillations at $F = 23.2$, $Q = 0.307$. (*b*) shows the wave probe, (*c*) the odd wavenumbers, and (*d*) the even wavenumbers.

terms of the eigenfunctions of the linear free-slip stability problem. These are simply products of Bessel functions with m-extrema across the radius, and Fourier harmonics with wavenumbers n in azimuth. The correction to the zonal flow ($n = 0$) is similarly expanded in Bessel functions of zeroth order except with vanishing circulation at $r = 1$ as a boundary condition.

Models of this type have been extensively investigated under the 'single-wave' assumption. Only one ($n = N$) wave is retained. Success with these models is achieved in the steady-wave regime, and in the amplitude vacillation in some circumstances. However, the transition to chaos, though occurring via a finite period-doubling, is predicted at a value of F that far exceeds the observed values for a particular Q (Hart 1986). One reason for this is that to get chaos or even periodic oscillations in such single-wave models it is necessary that the fixed points, representing steady waves, be unstable (or nearly so). The single-wave models tend to be similar to the classic three-component convection model of Lorenz (1963). But with top, bottom, and interfacial Ekman layers all included, the effective Prandtl number for the baroclinic flow is less than 2, unless F is quite large. Because the effective aspect here is about 1, the fixed points do indeed remain stable until F becomes very large. The critical value of the friction needed to destabilize the fixed points for wavenumber-1 disturbances and equal viscosities can be written (following Hart 1986) as

$$Q_c^2 = \frac{c^2 - c(2+2\mu) + 4\mu^2}{c^2 + 4c}. \tag{3}$$

Here c is related to the Froude number by

$$c = \mu(2+\epsilon),$$

with ϵ being the supercriticality

$$\epsilon = \frac{2F - \alpha^2}{\alpha^2}$$

The critical F, for linear inviscid disturbances, is related to the total wavenumber α by $F_c = 0.5\,\alpha^2$ so the smallest that ϵ can be is zero. The factor μ is a function of the relative magnitudes of top, bottom, and interfacial friction. It is equal to 1.0 if there

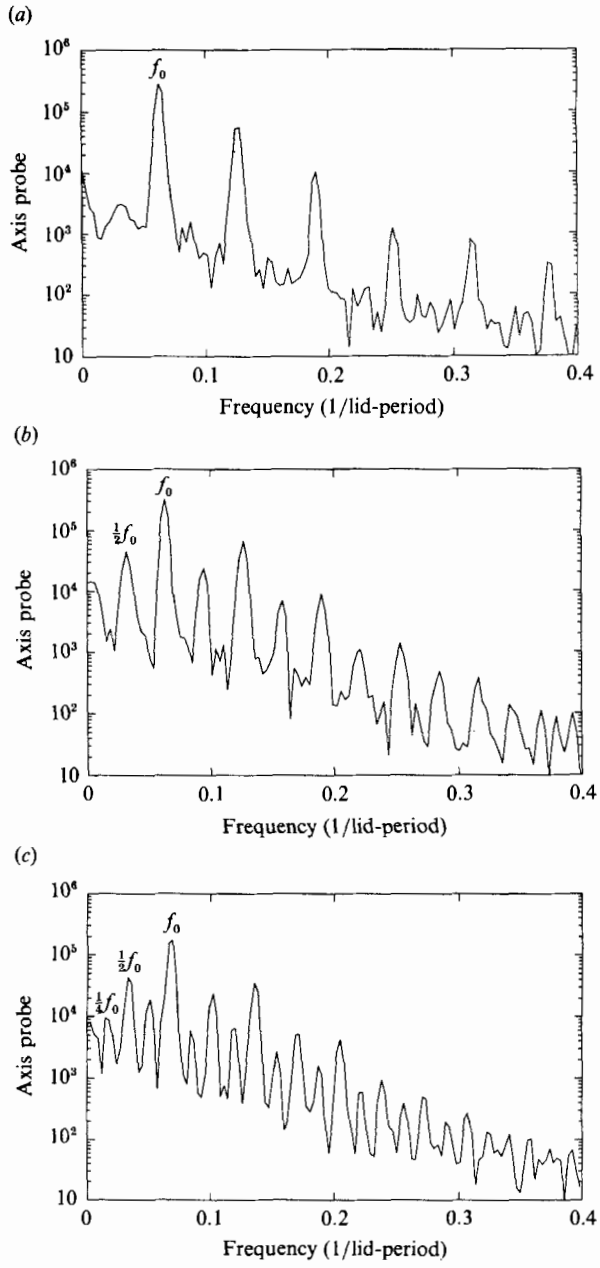

FIGURE 15(*a–c*). For caption see facing page.

is no interfacial friction, but is 0.5 if Ekman layers on both sides of the immiscible interface are included, with equal viscosities in both layers.

If $\mu = 1.0$ then c increases from 2.0 as the flow becomes supercritical. It is then easily seen from (3) that there always is a real value of Q_c for any value of ϵ, however small. However, if there is interfacial friction and $\mu = 0.5$, then c increases from 1 as ϵ becomes greater than zero. However the right-hand side of (3) is negative until $c = 2.618$. Thus the fixed points are stable until $\epsilon = 3.224$, or $F = 2.114\alpha^2$. This is roughly four times the critical values $F = F_c$ for $Q = 0$.

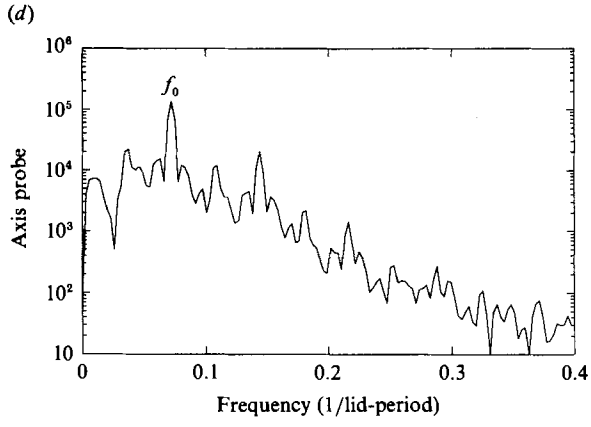

FIGURE 15. A sequence of spectra illustrating the period-doubling at $F = 23.2$. (*a*) $Q = 0.307$, (*b*) $Q = 0.297$, (*c*) $Q = 0.283$, (*d*) $Q = 0.271$.

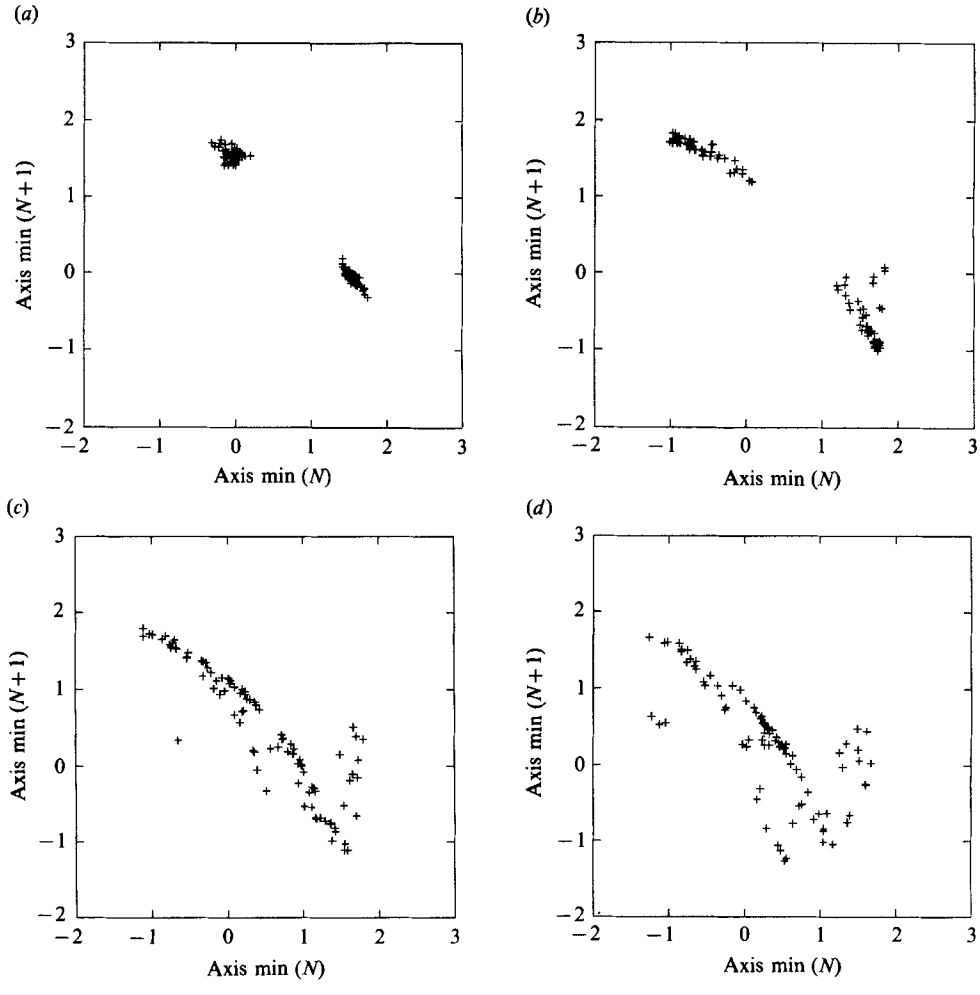

FIGURE 16. Axis-probe return maps for $F = 16.7$. (*a*) $Q = -0.0113$, (*b*) $Q = -0.0112$, (*c*) $Q = -0.0111$, (*d*) $Q = -0.0109$.

Q	$F = 17.3$	$F = 20.7$
−0.022	1.0±0.2	1.0
−0.020	1.0	1.8
−0.018	1.3	1.8
−0.015	1.3	2.0
−0.013	1.1	1.5
−0.010	1.5	> 2.5

TABLE 2. Zonal flow correlation dimensions D_2

In the experiments, chaos is observed at F of order 12, or about 1.7 times its inviscid critical value of $F_c = 6.88$ for $n = m = 1$. In order to get chaos or even periodicity in low-order models it is necessary to counter this severe effect of the number of dissipation layers on the stability of the flow. Of course, at four times the critical value a weakly nonlinear or single-wave expansion is not expected to work very well. Using multi-wave expansions Hart (1982), and more extensively, Pedlosky & Polvani (1987) argue that wave–wave interactions can be destabilizing. Because of this, and because we wanted to be sure to capture the interference vacillations which require more than one wave, as well as their nonlinear sidebands, we keep the six wavemodes (1, 1), (2, 1), (3, 1), (1, 2), (1,3), (2, 2) in the current computation. In these particular calculations the zonal flow is represented by 10 radial modes. Further increases in the zonal flow truncation had no effect on the bifurcations.

Figures 17 and 18 show the model regime diagrams for both types of forcing. The model runs were done by integrating the 44 nonlinear ordinary differential equations for the individual spectral amplitudes numerically, and by stepping Q as in the experiments. All fixed parameters had the experimental values from table 1. The model data were initially processed in the same manner as the experimental data. Comparing with figures 2 and 13, one may note the following overall behaviour of the model with respect to the laboratory experiments.

(i) For negative Q, the NIV regime is predicted very nicely. Within this regime the model behaviour mimics the experiment quite well (Ohlsen & Hart 1988, give further detail).

(ii) The chaotic regime occurs in the model in roughly the same position in parameter space. This is a major improvement over previous models which were much too stable. Unfortunately, the model transition is via quasi-periodicity. This is because the model does not kill off the NIV as $-Q$ decreases. There results, then, a mixture of amplitude vacillation and NIV in the QP model regime. The zonal attractor is a 2-torus. So also is the wave attractor (because the zonal and wave frequencies are related by integer multiples in NIV).

(iii) The model's chaotic region (C), is bounded on the low friction side by periodic motions, or even by steady flows at the lower F values. Although both the model and the experiments have periodic windows (many more can be observed in the model), this return to a periodic or steady regime is not found in the experiments.

(iv) The model fails to capture the experimentally observed phase-locked states for positive Q. The model signatures for easterly and westerly forcing are similar, while the experiment shows a strong asymmetry with respect to the sign of the Rossby number. Model chaos is again a combination of NIV and amplitude vacillations. Periodic windows appear in the chaotic regions, but these regions ultimately give way again to periodic or steady motions at small Q.

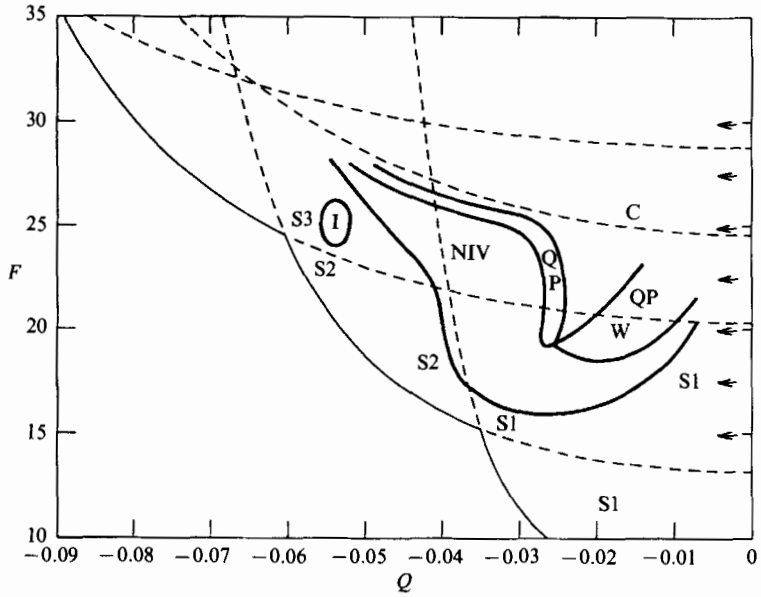

FIGURE 17. Six-wave model regime diagram for easterly forcing.

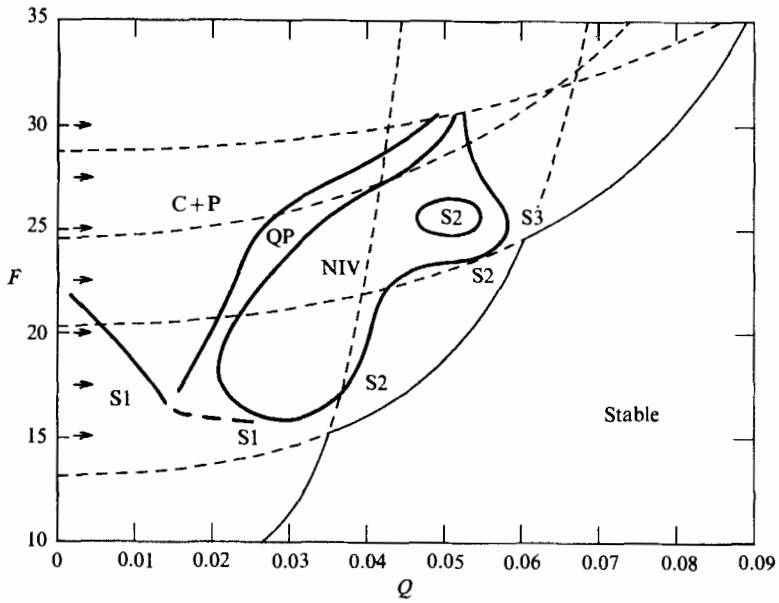

FIGURE 18. Six-wave model regime diagram for westerly forcing.

Figure 19 shows one example of the typical windowing phenomena in the model for $F = 22.5$. The successive minima of one of the model variables is plotted against Q, as small steps in this control parameter are made. This bifurcation diagram contains many regimes as Q decreases in magnitude towards zero, but only the major ones are shown in the figure. Interference vacillation period doubles, then becomes mixed with a low-frequency amplitude vacillation in a quasi-periodic regime. The first block of noisy-periodic chaos includes roughly equal spectral peaks from NIV and amplitude vacillation. When Q hits about -0.018 the amplitude vacillation dies

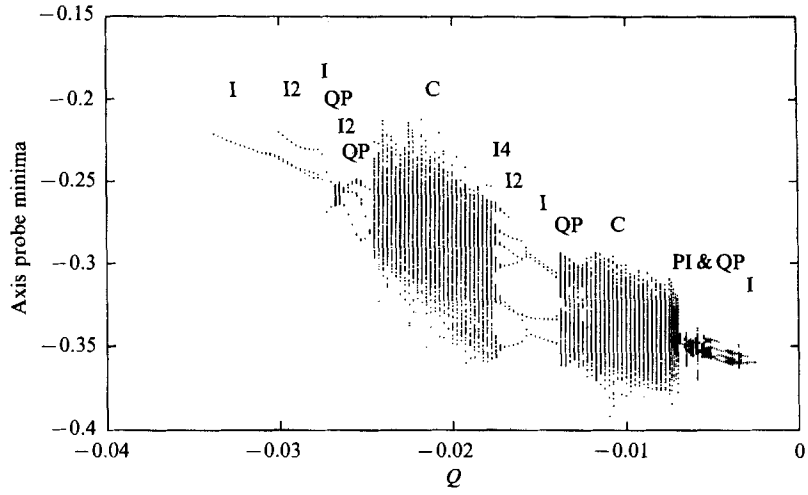

FIGURE 19. A typical bifurcation plot from the model for $F = 22.5$. I refers to period-1 nonlinear interference vacillation (NIV), In to period-n NIV, QP to quasi-periodic zonal flow, and C to chaotic zonal flow characterized by broad-band spectra and fuzzy tori.

out and the NIV reverse period-doubles to period-one. The second block of chaotic behaviour starts at about -0.014 and again involves a resurgence of amplitude vacillation. The Poincaré 'min-maps' for this transition show a beautiful wrinkling and fracturing of tori, leading to fuzzy tori. Although quite interesting, they are not presented here because the laboratory chaos is dominated by amplitude vacillation only. Furthermore, the final reverse cascade to periodicity at $Q \approx -0.006$ does not agree with experiments, which remain chaotic at small friction.

6. Conclusions

Laboratory experiments have been carried out illustrating the transition to chaos on the β-plane. For easterly forcing, steady waves give way to periodic 'nonlinear interference' vacillations related to mixed-wave dispersion and nonlinear sideband forcing of zonal flow oscillations. As the friction parameter Q is decreased in magnitude, the higher wavenumber in this mixed wave state dies out, and the remaining steady wave then breaks into an amplitude vacillation. This amplitude vacillation period-doubles to chaos, but other periodicities (even and odd) occur in narrow windows embedded in the chaotic regime. At very small friction (high driving), the chaos loses the noisy-periodic character typical of moderate forcing. For westerly forcing the nonlinear interference vacillations are less prominent, being replaced by amplitude vacillations with phase locking between the two dominant waves. The transition to chaos is similar to the easterly forcing case, and involves period-doubling of the amplitude vacillation. Periodic windows are again found in the low F, weakly chaotic regime. With westerly forcing, the transition to lower wavenumbers as Q is decreased, typical of the easterly-forced regimes at moderate F, does not occur.

The observed transition sequence of (possibly finite) period-doubling has occurred in models of baroclinic chaos (e.g. Hart 1986; Weng et al. 1986; Pedlosky & Polvani 1987). However, no models, including the six-wave one briefly discussed here, produce a good quantitative description of the observations. Perhaps we should not

expect a low-order model to accurately simulate baroclinic flows at order one supercriticality. The models are certainly useful in that basic interaction processes may be discerned, which sometimes have physical relevance to laboratory flows (e.g. the NIV). It may be, however, that important physical effects have been left out of the models. On the β-plane, the quasi-geostrophic equations are not invariant with respect to the direction of the forcing, as they are on the f-plane. However, the low-order model does not capture the observed qualitative difference between the easterly and westerly forcing. Perhaps the addition of horizontal shear (induced, for example, at the viscous sidewall, or by curvature effects at the top boundary or the interface where the Ekman suction velocity is not truly vertical) may remove this relative degeneracy in the model, partly because of the well-known direction-dependent shear flow stability condition involving a quantity like $U''-\beta$. The role of the rigid sidewall, and its effect on the waves and the zonal flow, needs both theoretical and experimental attention.

It is also possible that ageostrophic effects may be responsible for some of the differences between experiment and quasi-geostrophic models, especially in respect to the observed differences between easterly and westerly forcing. The internal Rossby number, based on the shear across the interface and using the experimental parameters, scales as

$$R_0 = \frac{0.0035}{Q}.$$

Near the experimental stable-to-unstable transition curves the Rossby number is quite small. From figure 2 it is seen that R_0 is less than 0.1 for all Froude numbers. However, in the NP and PW region at low F, R_0 can be as large as 0.3. Thus one interesting question is the effect of non-geostrophy on the nonlinear stability and saturation mechanisms in these flows.

It is hoped that the observations reported here will stimulate further work on this important problem, and will provide a useful data set for the verification of theories and models.

The authors thank the National Science Foundation for its support of the research reported here under its grant ATM-86-12736 to the University of Colorado.

REFERENCES

BARCILON, A. & DRAZIN, P. G. 1984 A weakly nonlinear theory of amplitude vacillation and baroclinic waves. *J. Atmos. Sci.* **41**, 3314–3330.

BUZYNA, G., PFEFFER, R. L. & KUNG, R. 1984 Transition to geostrophic turbulence in a rotating differentially heated annulus of fluid. *J. Fluid Mech.* **145**, 377–403.

GRASSBERGER, P. & PROCACCIA, I. 1983*a* Characterization of strange attractors. *Phys. Rev. Lett.* **50** 346–349.

GRASSBERGER, P. & PROCACCIA, I. 1983*b* Measuring the strangeness of strange attractors. *Physica* **9** D, 189–208.

GRASSBERGER, P. & PROCACCIA, I. 1983*c* Generalized dimensions of strange attractors. *Phys. Lett.* **97** A, 227–230.

HART, J. E. 1973 On the behavior of large amplitude baroclinic waves. *J. Atmos. Sci.* **30**, 1017–1034.

HART, J. E. 1981 Wavenumber selection in nonlinear baroclinic instability. *J. Atmos. Sci.* **38**, 400–408.

HART, J. E. 1982 Bifurcations in simple baroclinic flow. *Proc. 9th. Intl Congr. Appl. Mech. ASME* pp. 291–298.

HART, J. E. 1985 A laboratory study of baroclinic chaos on the f-plane. *Tellus* **37** A, 286–296.

HART, J. E. 1986 A model for the transition to baroclinic chaos. Physica **7** D, 350–362.

LINDZEN, R. S., FARREL, B. & JACQMIN, D. 1982 Vacillations due to wave interference: applications to the atmosphere and to annulus experiments. *J. Atmos. Sci.* **39**, 14–23.

LORENZ, E. N. 1963 Deterministic nonperiodic flow. *J. Atmos. Sci.* **20**, 130–141.

MANSBRIDGE, J. V. 1984 Wavenumber transition in baroclinically unstable flows. *J. Atmos. Sci.* **41**, 925–930.

MOROZ, I. M. & BRINDLEY, J. 1982 An example of two-mode interaction in a three-layer model of baroclinic instability. *Phys. Lett.* **91** A, 226–230.

OHLSEN, D. R. 1988 Nonlinear baroclinic instability on the Beta-plane. Ph.D. thesis, University of Colorado, 173 pp.

OHLSEN, D. R. & HART, J. E. 1988 Nonlinear interference vacillation. *Geophys. Astrophys. Fluid Dyn.* 25pp. In press.

PEDLOSKY, J. 1970 Finite-amplitude baroclinic waves. *J. Atmos. Sci.* **27**, 15–30.

PEDLOSKY, J. 1971 Finite-amplitude baroclinic waves with small dissipation. *J. Atmos. Sci.* **28**, 587–597.

PEDLOSKY, J. 1972 Limit cycles and unstable baroclinic waves. *J. Atmos. Sci.* **29**, 53–63.

PEDLOSKY, J. 1983 The effect of β on the chaotic behavior of unstable baroclinic waves. *J. Atmos. Sci.* **38**, 717–731.

PEDLOSKY, J. & POLVANI, L. M. 1987 Wave–wave interaction of unstable baroclinic waves. *J. Atmos. Sci.* **44**, 631–647.

PFEFFER, R. L. & FOWLIS, W. W. 1968 Wave dispersion in a rotating, differentially heated cylindrical annulus of fluid. *J. Atmos. Sci.* **25**, 361–371.

WENG, H.-Y., BARCILON, A. & MAGNON, J. 1986 Transitions between baroclinic flow regimes. *J. Atmos. Sci.* **43**, 1760–1777.